ORIGINAL RESEARCH

DNAH11 Localization in the Proximal Region of Respiratory Cilia Defines Distinct Outer Dynein Arm Complexes

Gerard W. Dougherty[1]*, Niki T. Loges[1]*, Judith A. Klinkenbusch[1], Heike Olbrich[1], Petra Pennekamp[1], Tabea Menchen[1], Johanna Raidt[1], Julia Wallmeier[1], Claudius Werner[1], Cordula Westermann[2], Christian Ruckert[3], Virginia Mirra[4], Rim Hjeij[1], Yasin Memari[5], Richard Durbin[5], Anja Kolb-Kokocinski[5], Kavita Praveen[6,7], Mohammad A. Kashef[8,9], Sara Kashef[8], Fardin Eghtedari[10], Karsten Häffner[11], Pekka Valmari[12], György Baktai[13], Micha Aviram[14], Lea Bentur[15], Israel Amirav[16], Erica E. Davis[6], Nicholas Katsanis[6], Martina Brueckner[17], Artem Shaposhnykov[18], Gaia Pigino[18], Bernd Dworniczak[3], and Heymut Omran[1]

[1]Department of General Pediatrics and [2]Gerhard-Domagk-Institut for Pathology, University Hospital Muenster, and [3]Department of Human Genetics, University of Muenster, Muenster, Germany; [4]Department of Translational Medical Sciences, Federico II University, Naples, Italy; [5]Wellcome Trust Sanger Institute, Cambridge, United Kingdom; [6]Center for Human Disease Modeling, Duke University, Durham, North Carolina; [8]Allergy Research Center, Shiraz University of Medical Sciences, Shiraz, Iran; [10]Australian Capital Territory Health, Canberra, Australian Capital Territory, Australia; [11]Department of General Pediatrics, Adolescent Medicine and Neonatology, University of Freiburg, Freiburg, Germany; [12]Department of Pediatrics, Lapland Central Hospital, Rovaniemi, Finland; [13]Department of Bronchology, Pediatric Institute Svábhegy, Budapest, Hungary; [14]Soroka Medical Center, Beer-Sheva, Israel; [15]Rambam Medical Center, Haifa, Israel; [16]Department of Pediatrics, University of Alberta, Edmonton, Alberta, Canada; [17]Department of Pediatrics, Yale University School of Medicine, New Haven, Connecticut; [18]Max Planck Institute of Molecular Cell Biology and Genetics, Dresden, Germany; [7]Regeneron Genetics Center, Tarrytown, New York; and [9]Baystate Medical Center, Springfield, Massachusetts

Abstract

Primary ciliary dyskinesia (PCD) is a recessively inherited disease that leads to chronic respiratory disorders owing to impaired mucociliary clearance. Conventional transmission electron microscopy (TEM) is a diagnostic standard to identify ultrastructural defects in respiratory cilia but is not useful in approximately 30% of PCD cases, which have normal ciliary ultrastructure. *DNAH11* mutations are a common cause of PCD with normal ciliary ultrastructure and hyperkinetic ciliary beating, but its pathophysiology remains poorly understood. We therefore characterized DNAH11 in human respiratory cilia by immunofluorescence microscopy (IFM) in the context of PCD. We used whole-exome and targeted next-generation sequence analysis as well as Sanger sequencing to identify and confirm eight novel loss-of-function *DNAH11* mutations. We designed and validated a monoclonal antibody specific to DNAH11 and performed high-resolution IFM of both control and PCD-affected human respiratory cells, as well as samples from green fluorescent protein (GFP)–left–right dynein mice, to determine the ciliary localization of DNAH11. IFM analysis demonstrated native DNAH11 localization in only the proximal region of wild-type human respiratory cilia and loss of DNAH11 in individuals with PCD with certain loss-of-function *DNAH11* mutations. GFP–left–right dynein mice confirmed proximal DNAH11 localization in tracheal cilia. DNAH11 retained proximal localization in respiratory cilia of individuals with PCD with distinct ultrastructural defects, such as the absence of outer dynein arms (ODAs). TEM tomography detected a partial reduction of ODAs in DNAH11-deficient cilia. *DNAH11* mutations result in a subtle ODA defect in only the proximal region of respiratory cilia, which is detectable by IFM and TEM tomography.

Keywords: left–right dynein; primary ciliary dyskinesia; normal ciliary ultrastructure; immunofluorescence microscopy; transmission electron microscopy

Clinical Relevance

Conventional transmission electron microscopy (TEM) is not diagnostic for approximately 30% of primary ciliary dyskinesia (PCD) cases because they have normal ciliary ultrastructure; *DNAH11* mutations are a common cause of PCD with normal ciliary ultrastructure and hyperkinetic ciliary beating, but its molecular characterization in human respiratory cilia is completely lacking. We show that DNAH11 distinctly localizes to the proximal region of respiratory cilia, independently of all previously described factors governing dynein arm assembly. TEM tomography detects a partial reduction of outer dynein arms in only the proximal region of DNAH11-deficient cilia. This helps explain why *DNAH11* mutations result in normal ciliary ultrastructure and hyperkinetic ciliary beating and suggests a novel mode of axonemal assembly in respiratory cilia.

(Received in original form October 30, 2015; accepted in final form February 2, 2016)

*These authors contributed equally to this work.

Am J Respir Cell Mol Biol Vol 55, Iss 2, pp 213–224, Aug 2016

Originally Published in Press as DOI: 10.1165/rcmb.2015-0353OC on February 24, 2016
Internet address: www.atsjournals.org

Primary ciliary dyskinesia (PCD; Mendelian Inheritance in Man or MIM no. 244400) is a recessively inherited disorder that affects at least 1 in 20,000 individuals (1). Individuals with PCD suffer from a chronic, destructive respiratory disorder characterized by bronchiectasis and progressive lung failure. This respiratory disorder results from defective mucociliary clearance, due to deficient ciliary beating of respiratory epithelial cells lining the airways (2). In almost half of individuals with PCD, left–right (LR) body patterning defects, such as *situs inversus*, are observed due to dysmotility of monocilia, which are present during early embryonic development at the LR organizer and produce a leftward fluid flow to establish body asymmetry (3). PCD is genetically heterogeneous, as mutations in over 30 distinct genes have been reported to cause this disease (*see* Table E1 in the online supplement). The majority of PCD-causing mutations result in gross ultrastructural defects of the respiratory ciliary axoneme that are detectable by transmission electron microscopy (TEM) analysis, such as the loss of outer dynein arms (ODAs) from mutations in *DNAH5* (4) and *DNAI2* (5) and microtubular disorganization with inner dynein arm (IDA) and nexin-link/dynein regulatory complex (N-DRC) defects from mutations in *CCDC39* (6) and *CCDC40* (7) (Figure 1). Indeed, TEM has been the gold standard to diagnose PCD (8) well before the first identification of mutations in a PCD-causing gene (9). In approximately 30% of PCD cases, however, there are no ultrastructural defects detectable by TEM (Figure 1), despite the clinical presentation of respiratory disease, including bronchiectasis and associated defects, such as *situs inversus*. The timely diagnosis of PCD and management of this respiratory disease may even be delayed in cases of normal ciliary ultrastructure without associated defects, such as *situs inversus* (10).

We and others have shown that mutations in the gene encoding *DNAH11* (MIM no. 611884) are a common cause of PCD with normal ciliary ultrastructure and a hyperkinetic beating pattern (11–14). We have established immunofluorescence microscopy (IFM) analysis of respiratory cilia as a complement to diagnostic measures, such as TEM and high-speed video microscopy analysis (HVMA), to identify axonemal defects of the ODAs and IDAs, as well as the N-DRC (5, 7, 15–17) and also tailored IFM to identify PCD variants with defective radial spoke (RS) head composure that do not exhibit gross ultrastructural abnormalities (18).

Studies addressing the molecular characterization of human DNAH11 in respiratory cilia, especially in the context of PCD, are completely lacking; only green fluorescent protein (GFP)-tagged mouse DNAH11 (GFP–left–right dynein [lrd]) localization has been shown previously (19). Therefore, we designed and validated a mouse monoclonal antibody specific to human DNAH11. Here, we show its specificity by matching its expression pattern with mouse GFP-DNAH11 (GFP-lrd) and confirming loss of DNAH11 in individuals with PCD with certain loss-of-function *DNAH11* mutations. We demonstrate that DNAH11, the ODA protein orthologous to the *Chlamydomonas* β heavy chain (HC), is restricted spatially to only the proximal region of respiratory ciliary axonemes, whereas its β-HC paralogue, DNAH9, is restricted to only the distal region of respiratory ciliary axonemes, thus defining two compositionally distinct ciliary regions. *DNAH11*-mutant respiratory cilia demonstrate characteristic stiffness and reduced ciliary bending in the proximal axonemal region by HVMA, indicating that DNAH11 function is essential for proper ciliary bending in this newly defined ciliary region. TEM tomography detected a partial reduction of ODAs in the proximal, but not distal, regions of cilia lacking DNAH11. We demonstrate further that DNAH11 localizes to respiratory ciliary axonemes independently of gross ultrastructural defects caused by mutations in genes encoding the ODA assembly factors, *DNAH5* and *DNAI2*, as well as the dynein axonemal assembly factors, *DNAAF1* and *DNAAF3*, suggesting that a subtle ODA defect accompanies *DNAH11* mutations, which is now detectable by IFM as well as TEM tomography.

Materials and Methods

Individuals with PCD

Signed and informed consent was received from patients fulfilling the diagnostic criteria of PCD and their family members, using protocols approved by the Institutional Ethics Review Board at the University of Muenster (Muenster, Germany) and collaborating institutions.

High-resolution immunofluorescence analyses of human respiratory cells were performed as described previously (5). Images were acquired using a Zeiss LSM 880 laser scanning microscope with Zen-2 software and Zeiss AxioObserver Z1 Apotome with AxioVision 4.8 software

This work was supported by funding from the Deutsche Forschungsgemeinschaft grants OL/450-1 (H. Olbrich) and OM 6/4, OM 6/7, and OM6/8 (H. Omran), Interdisziplinären Zentrum für Klinische Forschung Muenster grant Om2/009/12 (H. Omran), European Commission grant FP7/2007–2013 grant agreement (GA) 262,055 (Y.M. and H. Omran) as a Transnational Access project of the European Sequencing and Genotyping Infrastructure, EU-FP7 programs SYSCILIA GA 241,955 (H. Omran and N.K.), BESTCILIA GA 305,404 (H. Omran), Wellcome Trust grant WT098051 (R.D. and A.K.-K.), Chief Scientist Office of the Ministry of Health, Israel grant 3-6176 (I.A.), European Respiratory Society Long-Term Research Fellowship 2014-3574 (V.M.), and by U.S. National Institutes of Health grants DK072301 (N.K. and E.E.D.) and R01HL093280 (M.B.). N.K. is a distinguished George W. Brumley Professor.

Author Contributions: G.W.D. wrote the manuscript and performed immunofluorescence analysis with N.T.L., J.A.K., V.M., and R.H. and performed Sanger sequencing analysis with J.A.K. and H. Olbrich; G.W.D. and N.T.L. performed Western blotting and with H. Olbrich designed and characterized the anti–axonemal dynein heavy chain 11 antibody; P.P. and T.M. analyzed green fluorescent protein (GFP)–left–right dynein (lrd) mice; M.B. provided GFP-lrd mice and performed data analysis; C. Westermann performed transmission electron microscopy (TEM); J.R., J.W., C. Werner, and K.H. performed clinical analysis of patients with primary ciliary dyskinesia, including high-speed video microscopy; M.A.K., S.K., F.E., P.V., G.B., M.A., L.B., and I.A. provided clinical data; Y.M., R.D., and A.K.-K. performed whole-exome sequencing; C.R., K.P., E.E.D., N.K., and B.D. performed targeted next-generation sequencing and variant analysis; G.P. and A.S. performed TEM tomography; H. Omran designed and co-wrote the manuscript and analyzed all data.

Correspondence and requests for reprints should be addressed to Heymut Omran, M.D., University Children's Hospital Muenster, Department of General Pediatrics, Albert-Schweitzer-Campus 1, Muenster 48149, Germany. E-mail: heymut.omran@ukmuenster.de

This article has an online supplement, which is accessible from this issue's table of contents at www.atsjournals.org

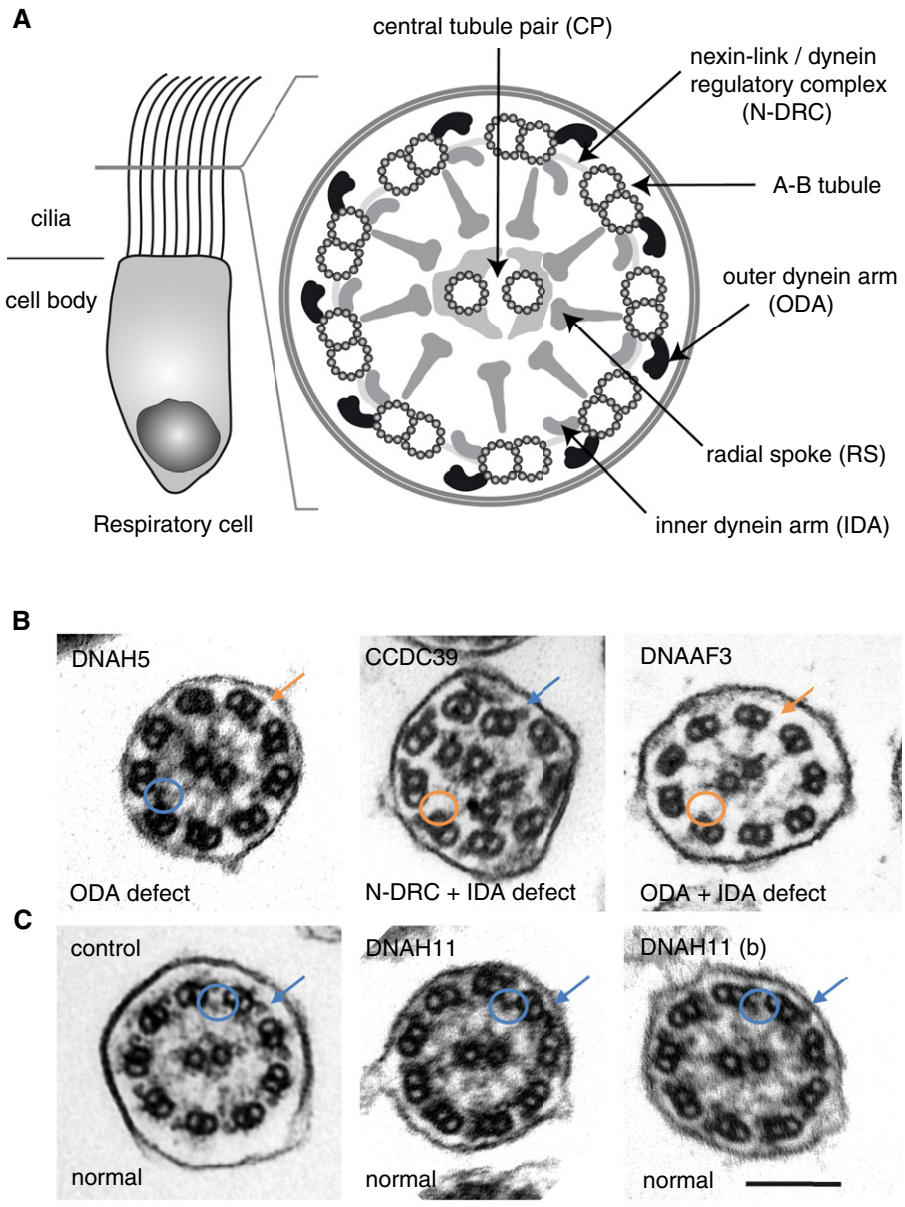

Figure 1. Diagnostic transmission electron microscopy (TEM) is not useful in approximately 30% of primary ciliary dyskinesia (PCD) cases. (*A*) Schematic of respiratory cell cilia and its cross-section highlighting the "9 + 2" organization of the ciliary axoneme and associated structures, as visualized by TEM. (*B*) TEM is diagnostic for loss of outer dynein arms (ODAs; e.g., *DNAH5* mutations), microtubular disorganization with nexin-link/dynein regulatory complex (N-DRC) and inner dynein arm (IDA) defects (e.g., *CCDC39* mutations), and loss of both ODAs and IDAs (e.g., *DNAAF3* mutations). (*C*) TEM is not diagnostic for *DNAH11* mutations, as they are indistinguishable from healthy control axonemes. *Blue arrows*, ODAs; *orange arrows*, absent ODAs; *blue circles*, IDAs; *orange circles*, absent IDAs. *Scale bar*: 100 nm. Individuals with PCD OI-16 II2 (DNAH5; p.Gln1464* hom.) and OP-1482 (*CCDC39*, c.610-2A>G hom.) were identified by whole-exome sequencing; the DNAH5, p.Gln1464* variant is novel and not present in the 1,000 Genomes and ExAC databases (sequencing data not shown); the *CCDC39*, c.610–2A>G variant was previously described (40). Individuals with PCD OP-98 II1 (DNAH11 p.Trp2604*, p.Ile4445Asnfs*3 het.) and OP-235 II2 (DNAH11 [*b*] p.Gln4233*, p.Leu4327Ser het.) as well as OP-989 II2 (DNAAF3, p.Leu108Pro hom.) were reported previously (14, 26).

(Carl Zeiss, Jena, Germany) and processed using Adobe CS4 software (Adobe Systems Incorporated, San Jose, CA).

TEM analysis, Western blotting, homozygosity mapping, haplotype analysis, and high-speed videomicroscopy analysis were performed as described previously (5, 16, 20, 21).

Whole-exome and sanger sequencing were performed as described previously (18). Variant analysis of whole-exome data was performed using Varbank software (Cologne Center of Genomics, Cologne, Germany). The *DNAH11* reference sequence is NM_001277115.1 (National Center for Biotechnology Information)/ENST00000409508 (Ensembl). Primer sequences used to confirm *DNAH11* mutations by Sanger sequencing are listed in the online supplement.

Additional information describing mouse monoclonal anti-DNAH11 antibody design and production, antibodies, DNAH11 (GFP-lrd) localization in mouse, TEM tomography, and next-generation DNA sequencing and variant analysis are available in the online supplement.

Results

Axonemal dynein HC proteins (e.g., DNAH5, DNAH9, and DNAH11) show a high degree of sequence conservation, especially in the centrally located motor domain region. To generate a specific anti-human DNAH11 antibody, we selected an epitope with low sequence conservation to other axonemal dynein HC proteins, specifically in the aminoterminal region of DNAH11 (Figure 2A; *see* also Figure E1). Because DNAH11 has been identified in the proteome of human respiratory cilia (22), and mouse GFP-DNAH11 has been shown to be localized in motile cilia (19), we prescreened anti-DNAH11 hybridoma lines by IFM for ciliary localization in human respiratory cells. Western blotting of lysates from porcine respiratory cells with anti-human DNAH11 (Figure 2B) demonstrated a cross-reactive, albeit weak, band of approximately 500 kD, consistent with the expected molecular weight of 520 kD. An immunoreactive band slightly below 500 kD may represent an isoform of DNAH11. Respiratory cells from healthy control individuals were costained with anti-DNAH11 and anti–α/β-tubulin. As

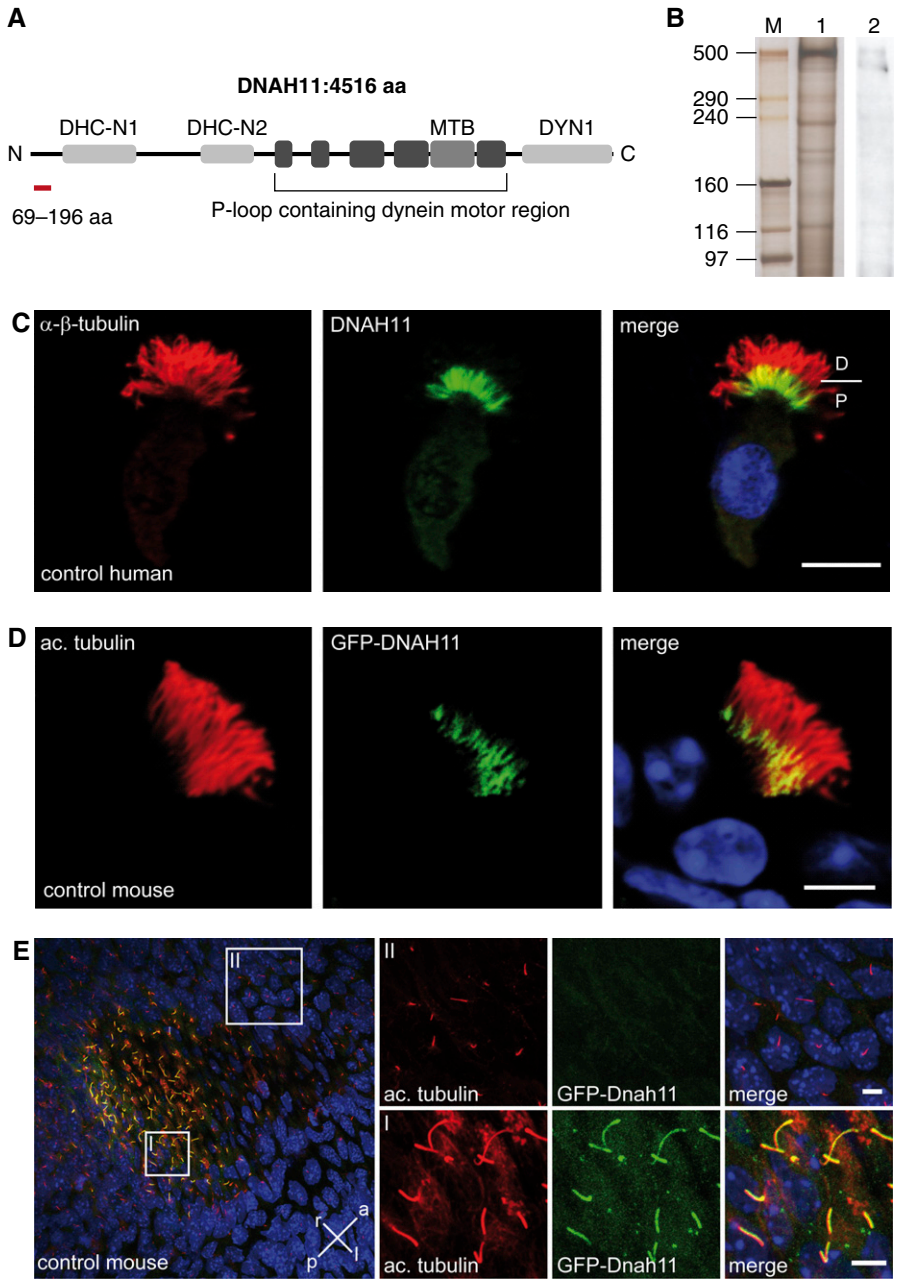

Figure 2. DNAH11 localizes exclusively to the proximal region of respiratory cilia. (*A*) Schematic of DNAH11 protein domains that are conserved among other DNAH proteins per the Conserved Domain Database. The P-loop region contains several ATPase domains as well as the microtubule binding (MTB) domain. DHC-N, dynein heavy chain, N-terminal region; DYN, dynein heavy chain/region D6 of dynein motor. *Red highlight*, the epitope of DNAH11 spanning amino acids 69–196. (*B*) Anti-DNAH11Western blotting of porcine axonemal extracts indicates immunoreactive bands of approximately 500 kD. M, marker lane; 1, silver stain of lysate; 2, anti-DNAH11. (*C*) Immunofluorescence microscopy (IFM) of human control respiratory cells shows that native DNAH11 (*green*) localizes to the proximal region of ciliary axonemes; α/β-tubulin (*red*) was used as counterstain to detect ciliary axonemes. D, distal; P, proximal; *scale bar*: 10 μm. (*D*) IFM of mouse respiratory cells expressing *green fluorescent protein (GFP)-DNAH11* (*GFP–left–right dynein* [*lrd*]) demonstrates that GFP-DNAH11 localizes to the proximal region of ciliary axonemes, similar to the pattern of human DNAH11 localization. Acetylated α-tubulin was used as counterstain to detect ciliary axonemes (*red*). *Scale bar*: 10 μm. (*E*) In contrast to mouse respiratory cilia, GFP-DNAH11 localizes throughout the entire axoneme in motile monocilia of the left–right organizer (*I*) in early mouse embryos but is not detectable in nonmotile cilia of the node or primary cilia of endodermal cells (*II*). Body axis is specified as right (*r*), left (*l*), anterior (*a*), and posterior (*p*). *Scale bars* in (*I*) and (*II*): 10 μm. ac., acetylated.

shown in Figure 2C, DNAH11 localized only to the proximal region of ciliary axonemes, as compared with panaxonemal localization of α/β-tubulin. We determined that a commercially available, polyclonal anti-DNAH11 antibody also identified DNAH11 in the proximal region of human respiratory cilia by IFM, and provided a robust cross-reactive signal by Western blotting of porcine axonemal extracts (*see* Figure E13). The mouse ortholog to DNAH11, also known as the lrd, was shown to be expressed in tissues containing motile cilia, including the LR organizer (19). Consistent with findings in human respiratory cells, mouse GFP-DNAH11 localized to the proximal region of respiratory cilia (Figure 2D). In contrast, mouse GFP-DNAH11 localization in monocilia of the LR organizer of GFP-lrd mice was panaxonemal rather than proximal (Figure 2E). These data demonstrate that human DNAH11 and mouse GFP-DNAH11 have a restricted, proximal localization in respiratory cilia, and that mouse GFP-DNAH11 has an unrestricted, panaxonemal localization pattern in the embryonic LR organizer; this distinction was not reported previously (19).

To validate the specificity of this anti-DNAH11 antibody, we examined individuals with PCD harboring novel loss-of-function *DNAH11* mutations. We identified a consanguineous Iranian family (OP-327) with five siblings, of whom four presented with recurrent upper and lower respiratory tract infections, and one also displayed *situs inversus totalis* (Figure 3A). Genome-wide linkage analysis of OP-327 identified chromosome 7 as the only genomic region with a significant logarithm of odds (LOD) score (above 3.0). Haplotype analysis demonstrated an 11.9-Mb region of homozygosity among the PCD siblings within the chromosomal interval 7p15.2–7p21.3 (physical positions 13,201,036–25,126,009; National Center for Biotechnology Information Map Viewer), consistent with homozygosity by descent. This genomic interval contains 136 genes, and the only known PCD-causing gene within this locus is *DNAH11* (Figure 3B). We subsequently analyzed DNA from OP-327 II4 by whole-exome sequencing and filtered pathogenic variants (Varbank software) located within this interval on chromosome 7. We identified a homozygous splice-site mutation in

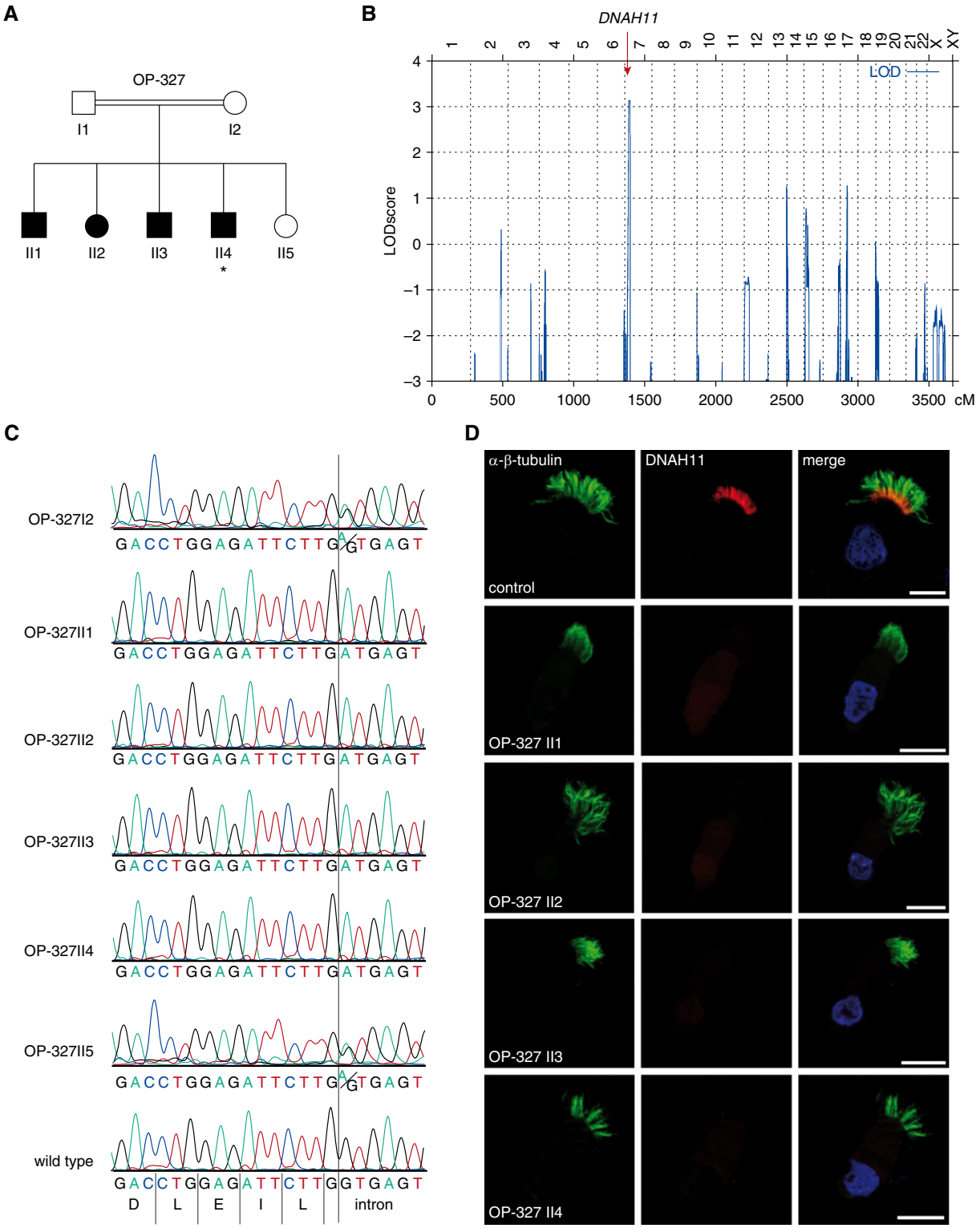

Figure 3. DNAH11 is absent in respiratory cilia of individuals with PCD with a homozygous *DNAH11* splice-site mutation. (*A*) Pedigree of the consanguineous PCD family OP-327. PCD siblings are shaded *black*, and the unaffected sibling is shaded *white*. **Situs inversus totalis*. (*B*) Genome-wide linkage analysis of family OP-327 indicates chromosome 7 (*x-axis* represents genomic position in centimorgans or cM) as the only significant logarithm of odds (LOD) score (*y-axis*); this genomic interval contains *DNAH11* (*red arrow*). (*C*) Sanger sequencing confirmed a homozygous splice donor variant in *DNAH11* (intron 73, c.11739 + 1G>A) in four PCD siblings (OP-327 II1–II4). The unaffected parent (OP-327 I2) and sibling (OP-327 II5) are heterozygous (A/G) for this variant, whereas wild-type DNA shows the G nucleotide at this position. The triplet nucleotide sequence (color) is shown above the translated amino acid sequence (*single letters*). (*D*) IFM shows that, in contrast to healthy human respiratory cells, DNAH11 (*red*) is absent in PCD siblings OP-327 II1–II4. α/β-tubulin (*green*) is used as counterstain to detect ciliary axonemes. *Scale bar*: 10 μm.

DNAH11 (c.11,739 + 1 G>A, intron 73); this variant affects a canonical donor splice-site, predicts aberrant splicing, and is absent from both the 1,000 Genomes and ExAC databases. We confirmed by Sanger sequencing that this homozygous *DNAH11* mutation was present in all affected siblings, but was heterozygous in the mother and unaffected sibling (DNA from the father was not available). Thus, segregation was consistent with autosomal recessive inheritance (Figure 3C). Next, we performed IFM on respiratory cells from all affected siblings using this anti-DNAH11 antibody and determined that DNAH11 was absent in respiratory cilia from these siblings (Figure 3D). These data demonstrate that the *DNAH11* c.11,739 + 1 G>A donor splice-site mutation results in the loss of DNAH11 and validated the specificity of this anti-DNAH11 antibody. Consistent with the reported *DNAH11*-mutant phenotype, the affected siblings had normal ciliary composition for the ODA HC protein DNAH5, the IDA light chain (LC) protein DNALI1, and the RS head protein (RSPH) 9, as determined by IFM (*see* Figure E2). Respiratory cells from the mother and unaffected sibling were not available for IFM; TEM and HVMA were not available for the affected siblings.

We examined DNAH11 localization in additional individuals with PCD with biallelic *DNAH11* mutations identified by either whole-exome or targeted next-generation sequencing (NGS) and verified by Sanger sequencing (*see* Table E2 and Figures E3–E7). All mutations were either absent or showed a frequency below 0.01 in the 1,000 Genomes and ExAC databases, and were scored as pathogenic (*see* Table E3). Consistent with classical loss-of-function *DNAH11* mutations in individuals with PCD OP-1250 II1 (exon 53, c.8698C>T, p.Arg2900* hom.) and OP-1324 II1 (exon 62, c.10036C>T, p.Arg3346* hom.), we found that DNAH11 was absent in respiratory cells from these individuals (Figures 4A–4C). TEM of both OP-1250 II1 and OP-1324 II1 showed normal ciliary ultrastructure (*see* Figures E3 and E4). Thus, anti-DNAH11 IFM can detect certain loss-of-function *DNAH11* mutations in cases with normal TEM. We next examined whether respiratory cells harboring either homozygous or compound heterozygous *DNAH11* missense mutations can exhibit aberrant DNAH11 localization, including respiratory cells from individuals with PCD OI-128 II2 (exon 81, c.13175C>T, p.Thr4392Met, hom.), OP-83 II2 (exon 27, c.4775G>T, p.Cys1592Phe; exon 52, c.8589C>G, p.Ser2863Arg), and OP-63 II2 (exon 52, c.8525G>A, p.Arg2842Gln; exon 52, c.8632C>T, p.Gln2878*) (Figures 4D–4F). Interestingly, we found that DNAH11 was also undetectable in these respiratory cilia, indicating that these *DNAH11*-mutant proteins are either not expressed or unable to be assembled in the ciliary axonemes. OI-128 II1 showed normal ciliary ultrastructure by TEM (*see* Figure E5). In contrast, IFM of respiratory cells from individuals with PCD OP-98 II1 (exon 48, c.7914G>C, p.Trp2604*; exon 82, c.13333_34insACCA, p.Ile4445Asnfs*3) and OP-235 II1 (exon 77, c.12697C>T, p.Gln4233*; exon 79, c.12980T>C, p.Leu4327Ser), which were reported previously (14), have normal ciliary ultrastructure by TEM (Figure 1C), and demonstrated normal proximal DNAH11 localization (*see* Figure E8). We conclude that anti-DNAH11 IFM can detect *DNAH11*-mutant cilia and therefore be helpful to establish the correct diagnosis (Figures 3D and 4A–4E; *see* also Figure E13). However, IFM is not always abnormal in individuals with PCD with *DNAH11* mutations (*see* Figure E8), demonstrating that certain *DNAH11* variants do not significantly alter DNAH11 protein expression and/or its assembly to the proximal ciliary region.

The ODAs are large, multisubunit molecular motors formed by the combined assembly of polypeptides of different sizes: HC (~400–500 kD), intermediate chain (~45–110 kD) and LC (~8–55 kD) (23, 24). In the unicellular alga, *Chlamydomonas*, the ODAs comprise three distinct HCs (α-, β-, and γ-HC). We reported previously that at least two distinct types of ODA complexes are present in human respiratory cilia (15): the ODA HC DNAH5 (orthologous to the *Chlamydomonas* γ-HC) is present throughout the entire length of the ciliary axoneme, whereas the ODA HC DNAH9 (orthologous to the *Chlamydomonas* β-HC) localizes exclusively to the distal ciliary compartment. Thus in respiratory cilia, at least two ODA types are present: type 1 (DNAH9 negative and DNAH5 positive; proximal ciliary axoneme) and type 2 (DNAH9 and DNAH5 positive; distal ciliary axoneme). To characterize further these ODA subtypes in human respiratory cilia, we costained control respiratory cells with anti-DNAH11 and anti-DNAH9. As shown in Figure 5, both DNAH11 and DNAH9 have distinct localization patterns in only the proximal or distal axonemal regions of respiratory cilia, respectively. This supports and clarifies our previous finding that distinct ODA subtypes are present in human respiratory cilia: a proximal axonemal region positive for DNAH11 (and negative for DNAH9, type 1), and a distal axonemal region positive for DNAH9 (and negative for DNAH11, type 2); DNAH5, which is localized along the entire respiratory axoneme, possibly functions as a heterodimeric dynein complex with the *Chlamydomonas* β-HC orthologs DNAH11 in the proximal region or with DNAH9 in the distal region. This proximal ciliary region containing DNAH11 is also distinct from the ciliary transition zone (*see* Figure E9). We next analyzed ciliary beating of *DNAH11*-mutant respiratory cells from individuals with PCD OP-1250 II1, OP-1324 II1, and OP-1324 II2 by HVMA. These respiratory cells characteristically exhibited reduced ciliary bending in the proximal (but not distal) region of the ciliary axonemes, subsequently reducing the amplitude of the waveform and manifesting as hyperkinetic beating (Figure 5D; *see* also Figure E10 and Videos E1–E8). We propose that loss or dysfunction of DNAH11 in the proximal region of respiratory cilia reduces dynein-mediated force generation in this area, resulting in reduced ciliary bending and increased stiffness in the proximal axonemal region.

To characterize further DNAH11 in diverse PCD subtypes, we examined respiratory cilia from individuals with PCD with defined genetic/phenotypic defects by IFM. Previous studies have demonstrated that loss-of-function mutations in the genes *DNAH5* and *DNAI2* (encoding structural components of type 1 and type 2 ODA complexes) result in lack of axonemal ODA assembly (4, 5, 15); these *DNAH5*- and *DNAI2*-mutant cilia are deficient for the ODA proteins, DNAH5, DNAH9, and DNAI2 (5, 15), and lack the ODA structure, as determined by TEM (Figure 1B). Interestingly, we found normal proximal DNAH11 localization in *DNAH5*- and *DNAI2*-mutant respiratory cilia,

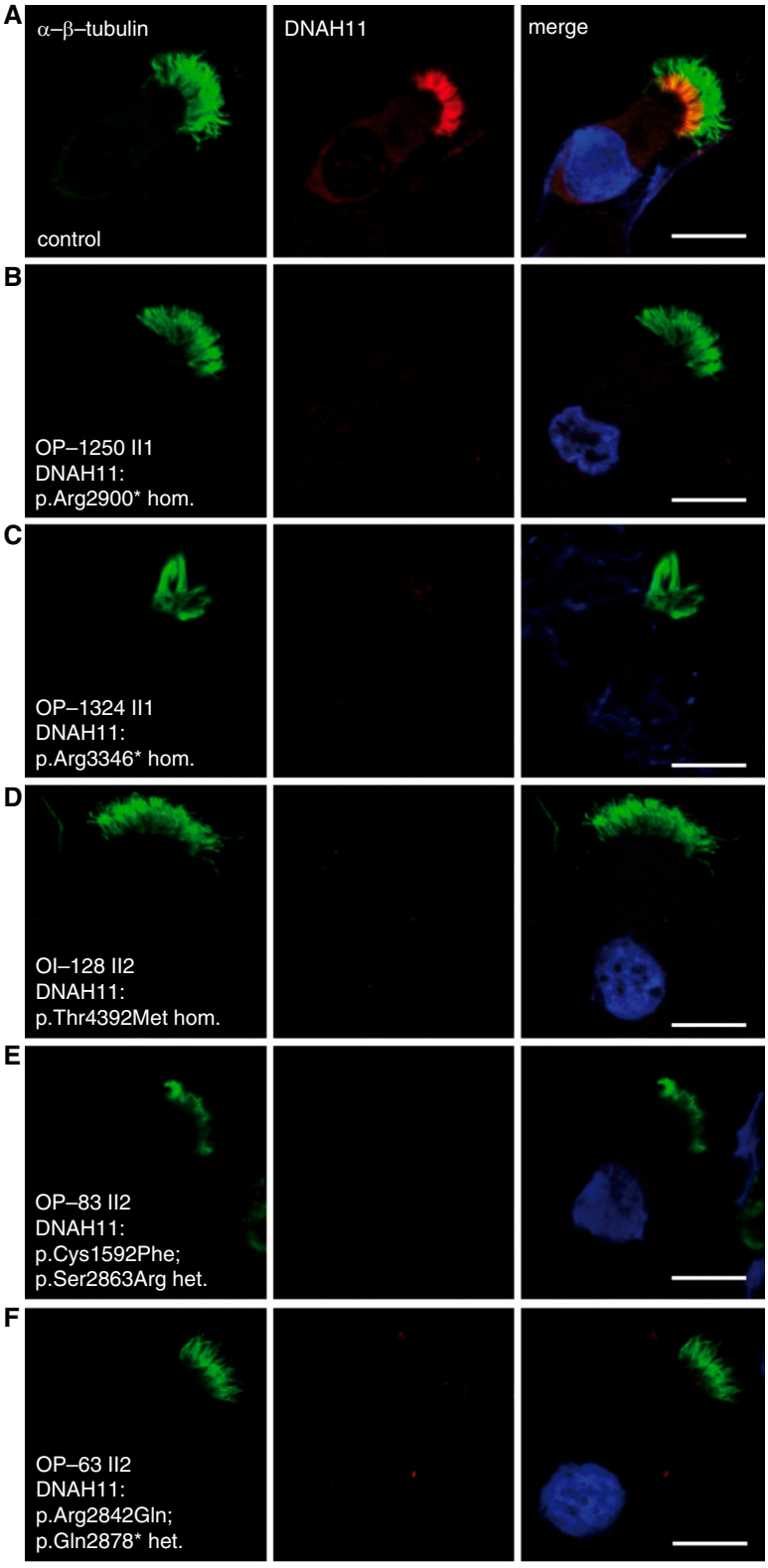

Figure 4. DNAH11 is absent in respiratory cilia of individuals with PCD with both homozygous nonsense and homozygous or compound heterozygous missense *DNAH11* mutations. We confirmed additional novel *DNAH11* loss-of-function mutations (*see* Figures E3–E7 and Tables E2 and E3) and determined that, in contrast to healthy control (*A*), these cilia lack DNAH11 (*B–F*). α/β-tubulin (*green*) is used as counterstain to detect ciliary axonemes. *Scale bars*: 10 μm.

indicating that the integrity of the ODA macromolecular complex is not essential for proximal DNAH11 assembly in respiratory axonemes (Figures 6A–6C). Previous studies have also demonstrated that loss-of-function mutations in *DNAAF1* (25) and *DNAAF3* (26) cause loss of both ODA and IDA assembly; *DNAAF1*- and *DNAAF3*-mutant cilia are deficient for the same ODA proteins as *DNAH5*- and *DNAI2*-mutant cilia, as well as the inner arm LC protein DNALI1, and they lack both the ODA and IDA structures, as determined by TEM (Figure 1B). We also observed normal proximal DNAH11 localization in these *DNAAF1*- and *DNAAF3*-mutant cilia (Figures 6D and 6E), demonstrating that the integrity of neither the ODA nor IDA macromolecular complex is essential for DNAH11 assembly in respiratory axonemes. Further supporting this observation, we also determined that DNAH11 retains proximal ciliary localization in *CCDC151*-mutant respiratory cilia, which also have ODA defects, due to functional loss of the ODA axonemal docking complex (27) (*see* Figure E11).

We next analyzed whether DNAH11 localization depends on the integrity of defined axonemal multiprotein complexes that intercalate with the A-B tubules, such as the N-DRC and RS structures (Figure 1A). We observed proximal DNAH11 localization in healthy control respiratory cilia as well as those harboring N-DRC (*CCDC164*-mutant cilia) (28), N-DRC and IDA (*CCDC39*-mutant cilia) (6), and RS (*RSPH4A*-mutant cilia lacking the entire RS head structure) (18) defects stemming from loss-of-function mutations in these respective PCD-causing genes (*see* Figures E11 and E12). We conclude that axonemal assembly of the β-HC ortholog, DNAH11, does not depend on the integrity of the N-DRC and RS ciliary complexes or the ODAs and IDAs in respiratory cilia.

Studies in the *Chlamydomonas* β-HC mutant, *oda*4-s7 (a truncated β-HC protein lacking its carboxyl terminus), have demonstrated a variable reduction in electron density in the midportion of ODAs and occasional reduction in ODA number by averaged TEM cross-section analysis (29–31). Therefore, we carefully re-evaluated the proximal region of *DNAH11*-deficient cilia (OP-1250 II1) by

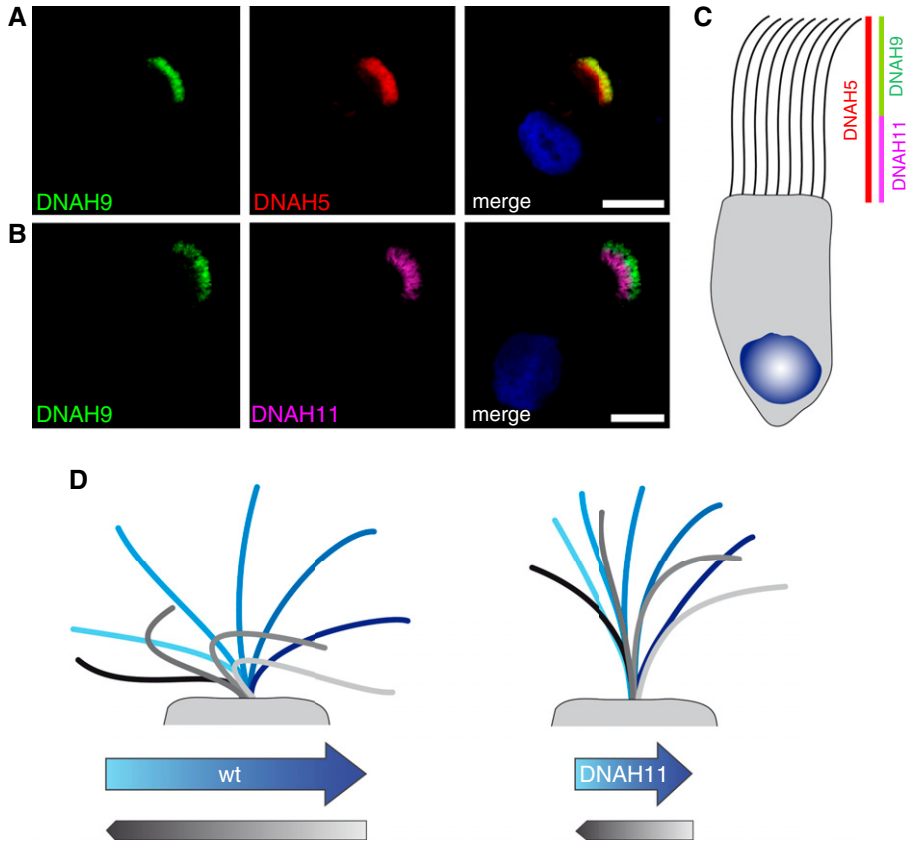

Figure 5. DNAH11 and DNAH9 distinctly localize to proximal and distal regions of respiratory cilia, respectively. (*A*) IFM shows that DNAH9 (*green*) localizes to the distal region of respiratory cilia; DNAH5 (*red*) localizes throughout the entire cilium. *Scale bar*: 10 μm. (*B*) IFM shows that DNAH11 (*purple*) localizes distinctly in the proximal region of respiratory cilia in contrast to DNAH9 (*green*), which localizes distinctly in the distal region of respiratory cilia. *Scale bar*: 10 μm. (*C*) A schematic shows that DNAH11 and DNAH9 localize to distinct regions in respiratory cilia, thus defining distinct proximal and distal ODA subtypes. (*D*) Model of hyperkinetic ciliary beating. Whereas healthy respiratory cilia display an average beat frequency of approximately 6 Hz, cilia from individuals with *DNAH11* mutations have an average beat frequency above 9 Hz, owing to reduced bending in the proximal ciliary region (*see* Figure E10 and Videos E1–E8). *Blue shades* indicate forward effective stroke; *gray shades* indicate recovery stroke. wt, wild type.

TEM tomography and detected a partial reduction in ODAs in the proximal, but not distal, ciliary region of these cilia (Figure 7). This indicates that *DNAH11*-mutant cilia harbor subtle ODA defects in only the proximal ciliary region, and clarifies the apparently normal ciliary ultrastructure of these cilia: this subtle ODA defect in *DNAH11*-mutant cilia may be easily overlooked by conventional TEM analysis (visualization of a single, structural projection in two dimensions), but is detectable by careful analysis of three-dimensional models of the proximal ciliary region obtained by TEM tomography (detailed visualization of a structure inside a reconstructed three-dimensional volume).

Discussion

The diagnosis of PCD in cases of normal ciliary ultrastructure and normal visceral arrangement (*situs solitus*) remains challenging and requires additional supportive assays (10). Despite several reports describing *DNAH11* mutations as a cause of PCD with normal ciliary ultrastructure, its molecular characterization and mechanistic contribution to this PCD subtype remains poorly understood. Here, we have validated a monoclonal antibody specific to DNAH11; DNAH11 is localized to the proximal region of respiratory cilia, and this is supported by the observation that GFP-DNAH11 is also localized proximally in mouse respiratory cilia. The differential localization pattern of GFP-DNAH11 between mouse respiratory cilia (restricted, proximal) and motile monocilia of the embryonic LR organizer (panaxonemal) underscores the observation that *DNAH11*/*Dnah11* mutations result in LR body patterning defects, and supports a critical function for DNAH11 in nodal ciliary beating (12, 14, 32–34).

Because *DNAH11* mutations are a common cause of PCD with normal ciliary ultrastructure, and conventional TEM is not useful in these cases, anti-DNAH11 IFM of respiratory cilia should facilitate diagnosis of this PCD subtype (Figures 3–4). However, we also show that some *DNAH11* mutations are compatible with axonemal assembly of a mutant DNAH11 protein (*see* Figure E8). This antibody likely would not detect carboxyl-terminal missense and/or truncating mutations (OP-98 II1, p.Ile4445Asnfs*3; OP-235 II2, p.Gln4233*, p.Leu4327Ser) unless they affect overall protein stability. Thus, a normal DNAH11 staining pattern using this antibody cannot rule out the presence of certain *DNAH11* mutations, and a negative DNAH11 staining pattern is not diagnostic *per se*. However, due to current limitations in routine genetic testing (e.g., low coverage, detection of indels), anti-DNAH11 IFM analysis could support a PCD diagnosis in unresolved genetic cases, for example, when only a single heterozygous *DNAH11* mutation is detected (14). We showed recently that IFM can help to establish a PCD diagnosis in cases with RS defects, using anti-RSPH1, RSPH4A, and RSPH9 antibodies (18). Furthermore, we have previously established IFM-based diagnostic screening to identify ODA defects using anti-DNAH5, anti-DNAH9, and anti-DNAI2 antibodies (5, 15, 16). We also showed that IFM using anti-CCDC39, anti-GAS8, and anti-DNALI1 antibodies can detect N-DRC and IDA defects (6, 7, 17, 25). Thus, the majority of known PCD types are now detectable by IFM, which is helpful to establish the correct diagnosis.

The restricted localization of human DNAH11 in the proximal region of respiratory cilia can help us to understand why *DNAH11* mutations result in PCD with hyperkinetic ciliary beating and reduced beating amplitude. A previous report that systematically analyzed ciliary beating of respiratory cilia (at 25°C) with

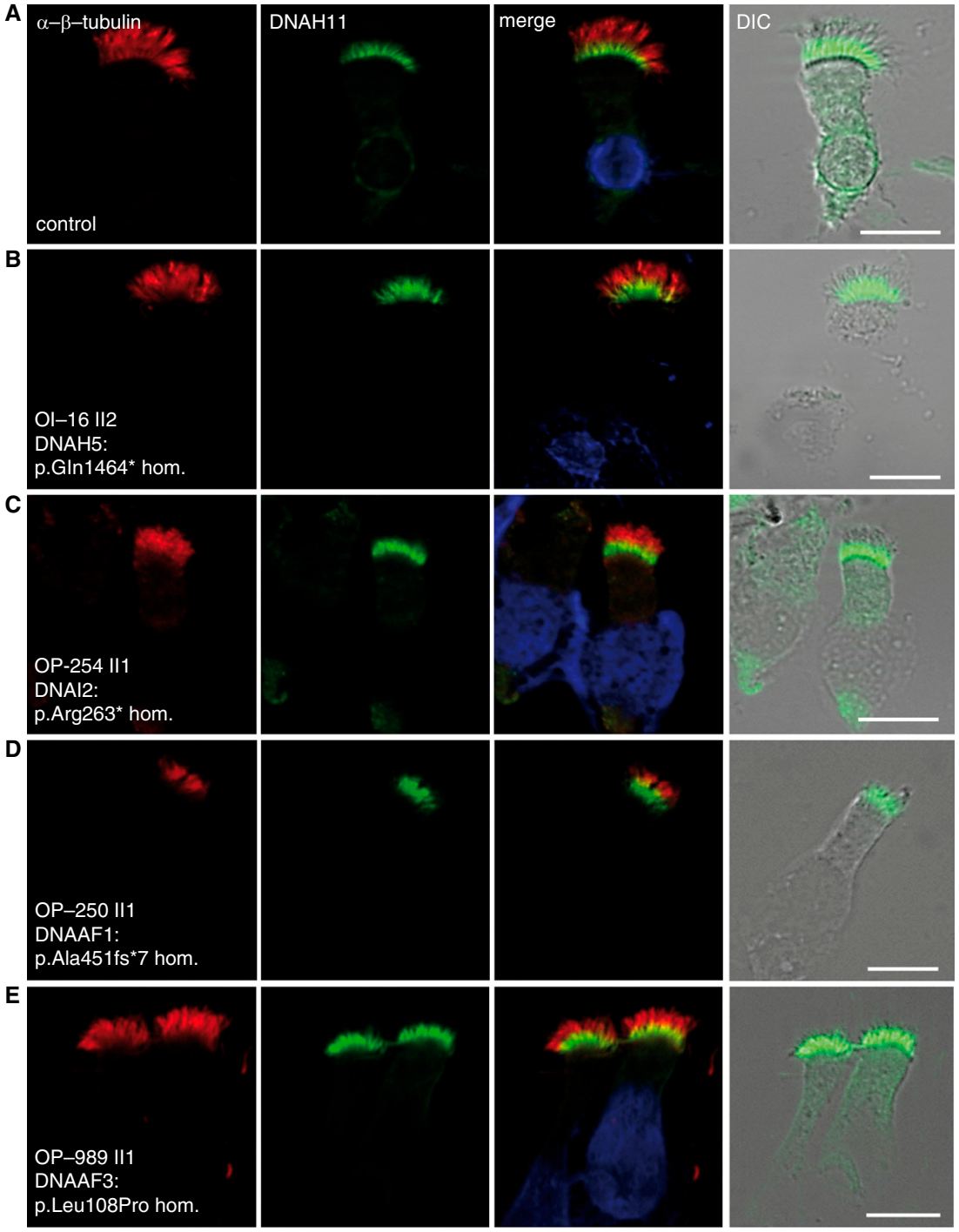

Figure 6. DNAH11 localizes to the proximal region of respiratory cilia in individuals with PCD with mutations affecting ODA and IDA assembly. Similar to healthy control respiratory cells (*A*), DNAH11 localizes to the proximal region of respiratory cilia in individuals with PCD harboring homozygous nonsense mutations in *DNAH5* (*B*) and *DNAI2* (*C*) that lack ODA structures, as well as individuals with PCD harboring homozygous loss-of-function mutations in *DNAAF1* (*D*) and *DNAAF3* (*E*) that lack both ODA and IDA structures. Anti-DNAH11 (*green*) is costained with α/β-tubulin (*red*) to detect ciliary axonemes. *Scale bar*: 10 μm. Individuals with PCD OP-254 II1, OP-250 II1 and OP-989 II1 were reported previously (5, 25, 26). TEM of OI-16 II2 and OP-989 II1 are shown in Figure 1B. DIC, differential interference contrast microscopy.

diverse genetic PCD variants (20) found that *DNAH11* mutations resulted in a higher ciliary beat frequency with a mean value of 8.7 Hz, in contrast to reported mean values for healthy controls (6.36 Hz) and respiratory disease controls (5.32 Hz). In contrast to other PCD variants, including those harboring ODA defects (e.g., *DNAH5* mutations), *DNAH11*-mutant respiratory cilia characteristically showed increased stiffness and reduced bending in the proximal axonemal region (*see* Videos

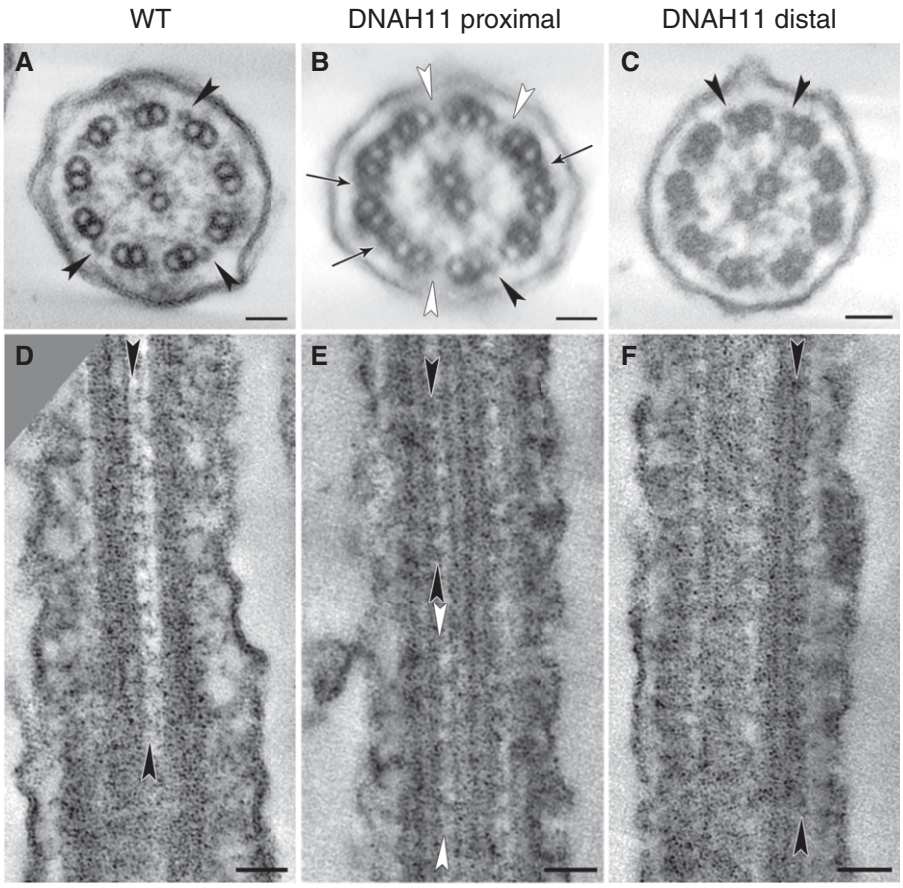

Figure 7. TEM tomography detects a partial reduction of ODAs in the proximal, but not distal, region of DNAH11-deficient cilia. Tomographic reconstruction of ciliary cross-sections from (*A*) wild-type (WT) and (*B* and *C*) DNAH11-deficient cilia (OP-1250 II1; *see* also Figure 4B and Figures E3 and E14, and Videos E1–E4) identify a partial reduction of ODAs (*white arrowheads*) in the proximal (*B*), but not distal (*C*), region of DNAH11-deficient cilia. *Black arrowheads*, structured ODAs; *black arrows* in *B* indicate the electron-dense material sometimes visible between microtubule doublets in the proximal ciliary region, approximately 400 nm distal to the transition zone and 100 nm distal to the base of the central pair microtubules. Tomographic reconstructions of ciliary longitudinal sections from (*D*) WT and (*E* and *F*) DNAH11-deficient cilia (OP-1250 II1) also identify a partial reduction of ODAs (*white arrowheads*) in the proximal (*E*), but not distal (*F*), region of DNAH11-deficient cilia. *Scale bars*: 50 nm.

E1–E8). The distinct proximal ciliary localization of DNAH11 and the characteristic beating deficiency observed in *DNAH11* mutations suggest that DNAH11 is critical for bending of the proximal ciliary region during the effective and recovery strokes of the ciliary beat cycle (Figure 5D). To our knowledge, this is the first study to describe a well defined compartment in the proximal region of respiratory cilia. Previous studies using *Chlamydomonas* have described proximal axonemal localization of IDA proteins, including dynein HC DHC11, the ortholog to human ciliary dynein HC DNAH7 (35, 36) and Fa2p, an ortholog to human NIMA–related kinase (NEK) family proteins (37). These studies also proposed a specialized role for the proximal axonemal region in bending and waveform initiation (35, 36), as well as mechanosensation and regulation of intraflagellar transport at the site of flagellar assembly/autotomy (37).

The *Chlamydomonas* β-HC gene show ambiguous BLAST homologies to three human genes: *DNAH9*, *DNAH11*, and *DNAH17*. This suggests that β-HC has diverged for specialized functions in higher eukaryotes during evolution. Our data demonstrate that certain differences between proximal type 1 ODAs and distal type 2 ODAs have evolved because β-HC DNAH9 assembly depends on the integrity of the ODA complex (5, 15, 25), whereas β-HC DNAH11 assembly does not (Figure 6; *see* also Figure E11). Recently, *in vitro* studies using *Chlamydomonas* demonstrated that β-HC is the main force generator coupled to ATP hydrolysis, in contrast to α-HC (for which there is no clear human ortholog) and γ-HC (human orthologs DNAH5 and DNAH8) (38). Although we cannot exclude a functional role for DNAH17 in respiratory cilia, it has not been identified in several transcriptomic and proteomic analyses of eukaryotic cilia (39), in contrast to both DNAH11 and DNAH9. Interestingly, anti-DNAH9 IFM analysis of both DNAH11-deficient (OP-1250 II1) and DNAH11-mutant (OP-235 II2) cilia demonstrated that the β-HC DNAH9 shifts from a distinctly distal to a panaxonemal localization (*see* Figure E14), in an identical distribution pattern to the γ-HC ortholog, DNAH5. Presumably, DNAH9 can heterodimerize with DNAH5 in the proximal ciliary region when DNAH11 is either defective or absent. However, DNAH9 cannot functionally replace the partial ODA defect in the proximal ciliary region (Figure 7) and characteristic hyperkinetic beating (Figure 5D; *see* also Figure E10 and Videos E1–E8) in *DNAH11*-mutant cilia. Based on our observation that DNAH11 and DNAH9 occupy distinct proximal and distal regions of respiratory cilia, we conclude that DNAH11 and DNAH9 are paralogs: DNAH11 has diverged from an ancestral β-HC as the principal effector of proximal ciliary bending in respiratory cilia, whereas DNAH9 functions in the distal axonemal region.

We and others have demonstrated previously that *DNAH11* mutations do not affect assembly of ODAs (12, 14). We now show by TEM tomography that a partial reduction of ODAs is detectable in only the proximal region of DNAH11-deficient cilia. In addition, we show by anti-DNAH11 IFM that the axonemal assembly of DNAH11 does not depend on the integrity of the macromolecular ODA and IDA complexes as well as the axonemal N-DRC and RS complexes. This demonstrates that the ODA defect underlying *DNAH11* mutations is subtle, and helps explain why these PCD cases demonstrate normal ciliary ultrastructure by conventional TEM. Furthermore, this predicts that a novel pathway of axonemal assembly and as-

yet unidentified genetic factors may be responsible for this relatively common (over 30%) PCD subtype.

In summary, these studies use a validated anti-DNAH11 antibody to define a distinct proximal region in respiratory cilia and provide insight into the pathophysiology of a common cause of PCD with normal ciliary ultrastructure and hyperkinetic ciliary beating. ■

Author disclosures are available with the text of this article at www.atsjournals.org.

Acknowledgments: The authors thank the individuals with primary ciliary dyskinesia and their families for participating in this study, and acknowledge the German patient support group "Kartagener Syndrom und Primaere Ciliaere Dyskinesie e.V." The authors also thank M. Herting, B. Lechtape, S. Fleige-Menzen, D. Ernst, L. Overkamp, K. Wohlgemuth, and F. J. Seesing for excellent technical assistance, G. Nürnberg and P. Nürnberg for homozygosity mapping data, and the Exome Aggregation Consortium for creating their exome variant database.

References

1. Werner C, Onnebrink JG, Omran H. Diagnosis and management of primary ciliary dyskinesia. *Cilia* 2015;4:2.
2. Fliegauf M, Benzing T, Omran H. When cilia go bad: cilia defects and ciliopathies. *Nat Rev Mol Cell Biol* 2007;8:880–893.
3. Pennekamp P, Menchen T, Dworniczak B, Hamada H. Situs inversus and ciliary abnormalities: 20 years later, what is the connection? *Cilia* 2015;4:1.
4. Olbrich H, Häffner K, Kispert A, Völkel A, Volz A, Sasmaz G, Reinhardt R, Hennig S, Lehrach H, Konietzko N, *et al*. Mutations in *DNAH5* cause primary ciliary dyskinesia and randomization of left–right asymmetry. *Nat Genet* 2002;30:143–144.
5. Loges NT, Olbrich H, Fenske L, Mussaffi H, Horvath J, Fliegauf M, Kuhl H, Baktai G, Peterffy E, Chodhari R, *et al*. *DNAI2* mutations cause primary ciliary dyskinesia with defects in the outer dynein arm. *Am J Hum Genet* 2008;83:547–558.
6. Merveille AC, Davis EE, Becker-Heck A, Legendre M, Amirav I, Bataille G, Belmont J, Beydon N, Billen F, Clément A, *et al*. CCDC39 is required for assembly of inner dynein arms and the dynein regulatory complex and for normal ciliary motility in humans and dogs. *Nat Genet* 2011;43:72–78.
7. Becker-Heck A, Zohn IE, Okabe N, Pollock A, Lenhart KB, Sullivan-Brown J, McSheene J, Loges NT, Olbrich H, Haeffner K, *et al*. The coiled-coil domain containing protein CCDC40 is essential for motile cilia function and left–right axis formation. *Nat Genet* 2011;43:79–84.
8. Afzelius BA. A human syndrome caused by immotile cilia. *Science* 1976; 193:317–319.
9. Pennarun G, Escudier E, Chapelin C, Bridoux AM, Cacheux V, Roger G, Clément A, Goossens M, Amselem S, Duriez B. Loss-of-function mutations in a human gene related to *Chlamydomonas reinhardtii* dynein IC78 result in primary ciliary dyskinesia. *Am J Hum Genet* 1999;65:1508–1519.
10. Kuehni CE, Frischer T, Strippoli MP, Maurer E, Bush A, Nielsen KG, Escribano A, Lucas JS, Yiallouros P, Omran H, *et al*.; ERS Task Force on Primary Ciliary Dyskinesia in Children. Factors influencing age at diagnosis of primary ciliary dyskinesia in European children. *Eur Respir J* 2010;36:1248–1258.
11. Bartoloni L, Blouin JL, Pan Y, Gehrig C, Maiti AK, Scamuffa N, Rossier C, Jorissen M, Armengot M, Meeks M, *et al*. Mutations in the *DNAH11* (axonemal heavy chain dynein type 11) gene cause one form of situs inversus totalis and most likely primary ciliary dyskinesia. *Proc Natl Acad Sci USA* 2002;99:10282–10286.
12. Schwabe GC, Hoffmann K, Loges NT, Birker D, Rossier C, de Santi MM, Olbrich H, Fliegauf M, Failly M, Liebers U, *et al*. Primary ciliary dyskinesia associated with normal axoneme ultrastructure is caused by *DNAH11* mutations. *Hum Mutat* 2008; 29:289–298.
13. Pifferi M, Michelucci A, Conidi ME, Cangiotti AM, Simi P, Macchia P, Boner AL. New *DNAH11* mutations in primary ciliary dyskinesia with normal axonemal ultrastructure. *Eur Respir J* 2010;35:1413–1416.
14. Knowles MR, Leigh MW, Carson JL, Davis SD, Dell SD, Ferkol TW, Olivier KN, Sagel SD, Rosenfeld M, Burns KA, *et al*.; Genetic Disorders of Mucociliary Clearance Consortium. Mutations of *DNAH11* in patients with primary ciliary dyskinesia with normal ciliary ultrastructure. *Thorax* 2012;67:433–441.
15. Fliegauf M, Olbrich H, Horvath J, Wildhaber JH, Zariwala MA, Kennedy M, Knowles MR, Omran H. Mislocalization of DNAH5 and DNAH9 in respiratory cells from patients with primary ciliary dyskinesia. *Am J Respir Crit Care Med* 2005;171: 1343–1349.
16. Hornef N, Olbrich H, Horvath J, Zariwala MA, Fliegauf M, Loges NT, Wildhaber J, Noone PG, Kennedy M, Antonarakis SE, *et al*. *DNAH5* mutations are a common cause of primary ciliary dyskinesia with outer dynein arm defects. *Am J Respir Crit Care Med* 2006;174: 120–126.
17. Omran H, Kobayashi D, Olbrich H, Tsukahara T, Loges NT, Hagiwara H, Zhang Q, Leblond G, O'Toole E, Hara C, *et al*. Ktu/PF13 is required for cytoplasmic pre-assembly of axonemal dyneins. *Nature* 2008; 456:611–616.
18. Frommer A, Hjeij R, Loges NT, Edelbusch C, Jahnke C, Raidt J, Werner C, Wallmeier J, Große-Onnebrink J, Olbrich H, *et al*. Immunofluorescence analysis and diagnosis of primary ciliary dyskinesia with radial spoke defects. *Am J Respir Cell Mol Biol* 2015;53:563–573.
19. McGrath J, Somlo S, Makova S, Tian X, Brueckner M. Two populations of node monocilia initiate left–right asymmetry in the mouse. *Cell* 2003;114:61–73.
20. Raidt J, Wallmeier J, Hjeij R, Onnebrink JG, Pennekamp P, Loges NT, Olbrich H, Häffner K, Dougherty GW, Omran H, *et al*. Ciliary beat pattern and frequency in genetic variants of primary ciliary dyskinesia. *Eur Respir J* 2014;44:1579–1588.
21. Olbrich H, Schmidts M, Werner C, Onoufriadis A, Loges NT, Raidt J, Banki NF, Shoemark A, Burgoyne T, Al Turki S, *et al*.; UK10K Consortium. Recessive *HYDIN* mutations cause primary ciliary dyskinesia without randomization of left–right body asymmetry. *Am J Hum Genet* 2012;91:672–684.
22. Ostrowski LE, Blackburn K, Radde KM, Moyer MB, Schlatzer DM, Moseley A, Boucher RC. A proteomic analysis of human cilia: identification of novel components. *Mol Cell Proteomics* 2002;1: 451–465.
23. Ibañez-Tallon I, Heintz N, Omran H. To beat or not to beat: roles of cilia in development and disease. *Hum Mol Genet* 2003;12: R27–R35.
24. King SM. Integrated control of axonemal dynein AAA^{+} motors. *J Struct Biol* 2012;179:222–228.
25. Loges NT, Olbrich H, Becker-Heck A, Häffner K, Heer A, Reinhard C, Schmidts M, Kispert A, Zariwala MA, Leigh MW, *et al*. Deletions and point mutations of *LRRC50* cause primary ciliary dyskinesia due to dynein arm defects. *Am J Hum Genet* 2009; 85:883–889.
26. Mitchison HM, Schmidts M, Loges NT, Freshour J, Dritsoula A, Hirst RA, O'Callaghan C, Blau H, Al Dabbagh M, Olbrich H, *et al*. Mutations in axonemal dynein assembly factor DNAAF3 cause primary ciliary dyskinesia. *Nat Genet* 2012;44:381–389, S1–S2.
27. Hjeij R, Onoufriadis A, Watson CM, Slagle CE, Klena NT, Dougherty GW, Kurkowiak M, Loges NT, Diggle CP, Morante NF, *et al*.; UK10K Consortium. *CCDC151* mutations cause primary ciliary dyskinesia by disruption of the outer dynein arm docking complex formation. *Am J Hum Genet* 2014;95:257–274.
28. Wirschell M, Olbrich H, Werner C, Tritschler D, Bower R, Sale WS, Loges NT, Pennekamp P, Lindberg S, Stenram U, *et al*. The nexin–dynein regulatory complex subunit DRC1 is essential for motile cilia function in algae and humans. *Nat Genet* 2013;45:262–268.

29. Sakakibara H, Takada S, King SM, Witman GB, Kamiya R. A *Chlamydomonas* outer arm dynein mutant with a truncated beta heavy chain. *J Cell Biol* 1993;122:653–661.
30. Liu Z, Takazaki H, Nakazawa Y, Sakato M, Yagi T, Yasunaga T, King SM, Kamiya R. Partially functional outer-arm dynein in a novel *Chlamydomonas* mutant expressing a truncated gamma heavy chain. *Eukaryot Cell* 2008;7:1136–1145.
31. Takazaki H, Liu Z, Jin M, Kamiya R, Yasunaga T. Three outer arm dynein heavy chains of *Chlamydomonas reinhardtii* operate in a coordinated fashion both *in vitro* and *in vivo*. *Cytoskeleton (Hoboken)* 2010;67:466–476.
32. Hummel KP, Chapman DB. Visceral inversion and associated anomalies in the mouse. *J Hered* 1959;50:9–13.
33. Supp DM, Witte DP, Potter SS, Brueckner M. Mutation of an axonemal dynein affects left–right asymmetry in inversus viscerum mice. *Nature* 1997;389:963–966.
34. Supp DM, Brueckner M, Kuehn MR, Witte DP, Lowe LA, McGrath J, Corrales J, Potter SS. Targeted deletion of the ATP binding domain of left–right dynein confirms its role in specifying development of left–right asymmetries. *Development* 1999;126:5495–5504.
35. Yagi T, Uematsu K, Liu Z, Kamiya R. Identification of dyneins that localize exclusively to the proximal portion of *Chlamydomonas flagella*. *J Cell Sci* 2009;122:1306–1314.
36. Bui KH, Yagi T, Yamamoto R, Kamiya R, Ishikawa T. Polarity and asymmetry in the arrangement of dynein and related structures in the *Chlamydomonas axoneme*. *J Cell Biol* 2012;198:913–925.
37. Mahjoub MR, Qasim Rasi M, Quarmby LM. A NIMA-related kinase, Fa2p, localizes to a novel site in the proximal cilia of *Chlamydomonas* and mouse kidney cells. *Mol Biol Cell* 2004;15:5172–5186.
38. Furuta A, Yagi T, Yanagisawa HA, Higuchi H, Kamiya R. Systematic comparison of *in vitro* motile properties between *Chlamydomonas* wild-type and mutant outer arm dyneins each lacking one of the three heavy chains. *J Biol Chem* 2009;284:5927–5935.
39. Gherman A, Davis EE, Katsanis N. The ciliary proteome database: an integrated community resource for the genetic and functional dissection of cilia. *Nat Genet* 2006;38:961–962.
40. Antony D, Becker-Heck A, Zariwala MA, Schmidts M, Onoufriadis A, Forouhan M, Wilson R, Taylor-Cox T, Dewar A, Jackson C, *et al*.; Uk10k. Mutations in *CCDC39* and *CCDC40* are the major cause of primary ciliary dyskinesia with axonemal disorganization and absent inner dynein arms. *Hum Mutat* 2013;34:462–472.